Xujun LYU, Long DI, Zongli LIN, 2019. On robustness of an AMB suspended energy storage flywheel platform under characteristic model based all-coefficient adaptive control laws. *Frontiers of Information Technology & Electronic Engineering,* 20(1):120-130. https://doi.org/10.1631/FITEE.1800606

On robustness of an AMB suspended energy storage flywheel platform under characteristic model based all-coefficient adaptive control laws

Key words: Intelligent control; Robustness; Uncertainty; Disturbance rejection; Active magnetic bearings; Energy storage flywheels

Corresponding author: Xujun LYU
E-mail: lyuxujun@mail.hzau.edu.cn
 ORCID: https://orcid.org/0000-0002-2466-2338

Motivation (1/5)

- Flywheels

$$E = \frac{1}{2} J_{\mathrm{p}} \omega^2$$

E : stored energy;

J_{p} : polar moment of inertia;

ω : angular speed.

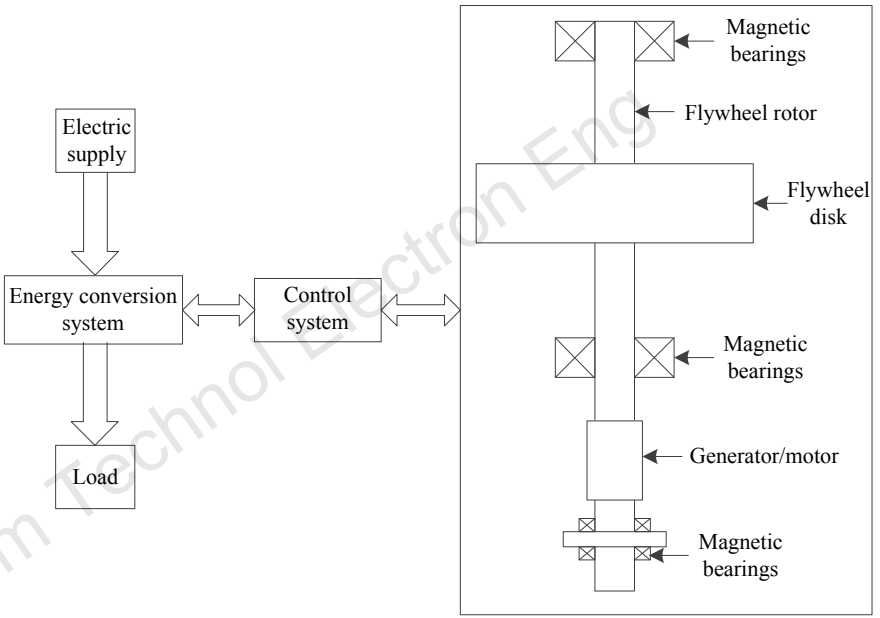

- Literature review

The complexity of AMB suspended flywheel systems → Test rigs → Too costly

The absence of past operational data → The implementation of control designs → Too difficult

We recently developed an experimental platform for AMB suspended energy storage flywheel in the Rotating Machinery and Controls (ROMAC) Laboratory, University of Virginia (Lyu, et al., 2016).

Motivation (2/5)

- Literature review (Cont'd)

The classical PID control design method → Easy to implement but not effective in handling complex rotordynamics

Modern control theory (H_∞ and μ-synthesis) → Usually requires a plant model and an accurate characterization of the uncertainties

Di and Lin (2014) explored the application of characteristic model based all-coefficient adaptive control (ACAC), originally proposed by Wu et al. (2007, 2009). → Resulting in lower levels of vibration than that of a benchmark μ-synthesis controller

We implemented the characteristic model based all-coefficient adaptive control (ACAC) on the platform mentioned above (Lyu, et al., 2018). Despite its simplicity, the characteristic model based ACAC can achieve a strong control performance according to both simulation and experimental results.

Motivation (3/5)

- AMB suspended flywheel test rig

$$M\ddot{q} + (C + \Omega G)\dot{q} + Kq = B_{\mathrm{m}}F_{\mathrm{mag}} + B_{\mathrm{e}}F_{\mathrm{ext}}, \quad (1)$$

where M is the symmetric flywheel rotor mass matrix, C the symmetric damping matrix, G the skew-symmetric gyroscopic effect matrix, K the symmetric stiffness matrix, Ω the rotational speed, B_{m} the position distribution matrix of the support AMBs, F_{mag} the forces provided by support AMBs, B_{e} the position distribution matrix of the external forces, F_{ext} the external forces acting on the rotor, and q the generalized displacement vector.

Motivation (4/5)

- AMB suspended flywheel test rig (Cont'd)

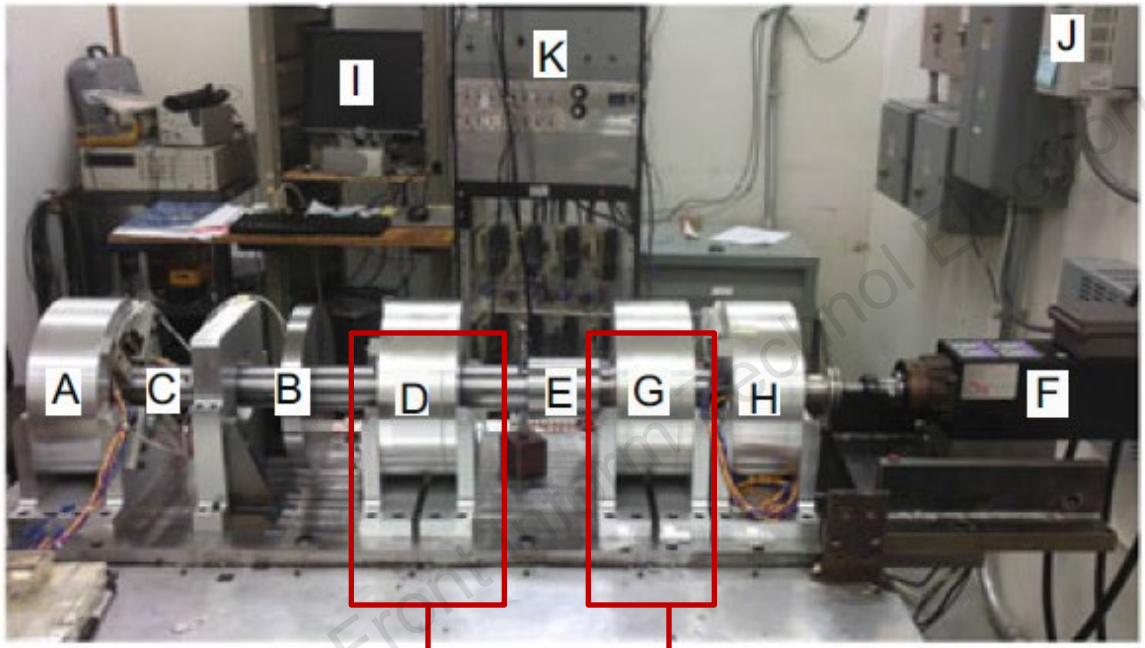

A: non-driven end support AMB
C: rotor shaft
E: gyroscopic disk 2
G: quarter-span disturbance AMB
I: control station
K: amplifiers and sensor conditioning station

B: gyroscopic disk 1
D: mid-span disturbance AMB
F: electric motor
H: driven end support AMB
J: variable frequency drive

To emulate the operation of an energy storage flywheel

Fig. 1 A flexible rotor-AMB test rig

Motivation (5/5)

- AMB suspended flywheel test rig (Cont'd)

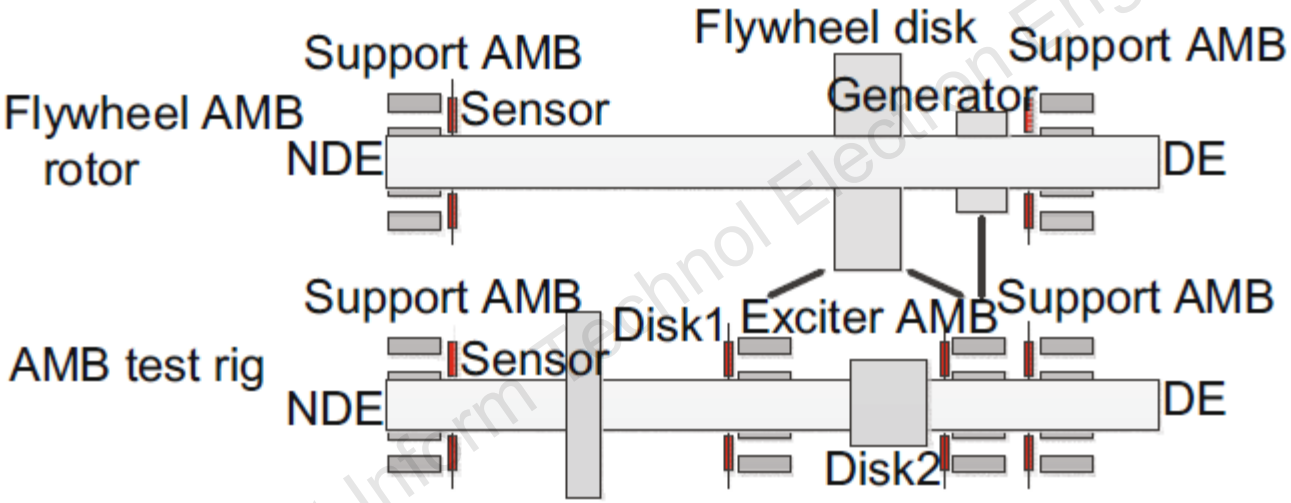

Fig. 2 Schematic of the experimental platform for AMB suspended flywheels

The exciter AMB at the quarter span → To emulate the negative stiffness induced by the generator

Two exciter AMBs at the mid-span and the quarter-span → To generate gyroscopic coupling resulting from the flywheel disk

Main idea

To examine the robustness of the characteristic model based ACAC on the AMB suspended energy storage flywheel platform with respect to:

1. plant uncertainties;

2. external disturbances;

3. time delay.

Method (1/3)

- The characteristic model based ACAC

Overview of the closed-loop system:

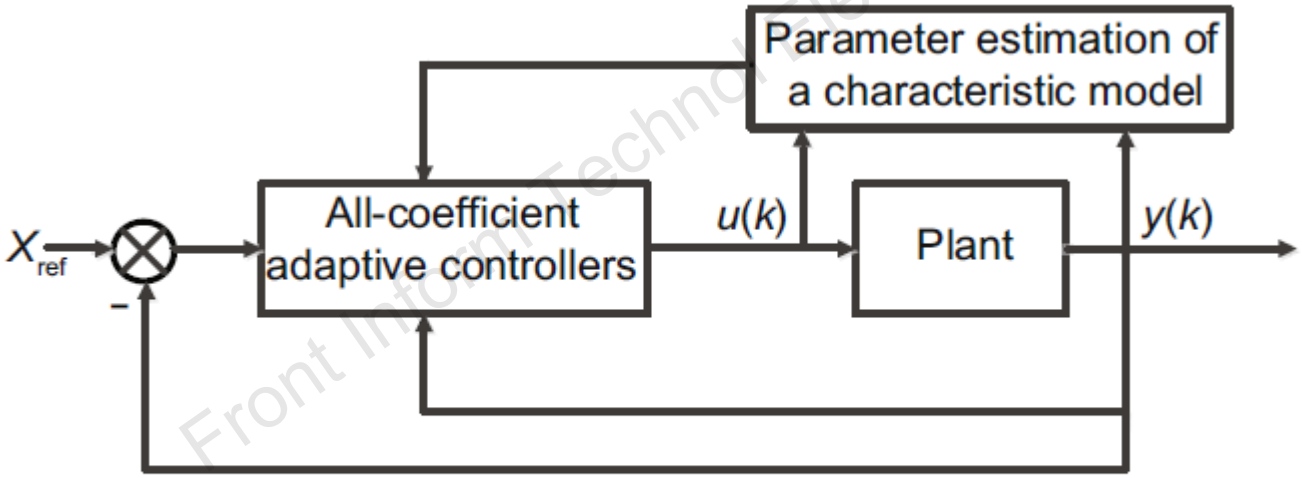

Fig. 3 Diagram of the characteristic model based ACAC system

Method (2/3)

- The characteristic model based ACAC (Cont'd)

Characteristic modeling:

Considering a linear time-invariant plant described as

$$G(s) = \frac{b_m s^m + b_{m-1} s^{m-1} + \ldots + b_1 s + b_0}{s^n + a_{n-1} s^{n-1} + \ldots + a_1 s + a_0},$$

If the control objective is position keeping or reference tracking, and the sampling period T is sufficiently small

$$\begin{aligned} y(k) =& f_1(k) y(k-1) + f_2(k) y(k-2) \\ &+ g_0(k) u(k-1) + g_1(k) u(k-2), \end{aligned} \quad (3)$$

where $u(k)$ is the control input, $y(k)$ the system output, and $f_1(k)$, $f_2(k)$, $g_0(k)$, and $g_1(k)$ the characteristic parameters

Method (3/3)

- The characteristic model based ACAC (Cont'd)

The controller

$$u_c(k) = u_O(k) + u_G(k) + u_D(k) + u_I(k),$$

Maintaining/tracking control :

$$u_O(k) = \frac{y_r(k) - \hat{f}_1(k)y(k) - \hat{f}_2(k)y(k-1) - \hat{g}_1(k)u_O(k-1)}{\hat{g}_0(k) + \lambda_1},$$

Golden section adaptive control :

$$u_G(k) = \frac{l_1\hat{f}_1(k)\tilde{y}(k) + l_2\hat{f}_2(k)\tilde{y}(k-1) + \hat{g}_1(k)u_G(k-1)}{\hat{g}_0(k) + \lambda_1},$$

Differential control:

$$u_D(k) = d_1\frac{\tilde{y}(k) - \tilde{y}(k-1)}{T},$$

Integral control:

$$u_I(k) = d_1\frac{\tilde{y}(k) - \tilde{y}(k-1)}{T},$$

where $y_r(k)$ is the reference output, λ_1 is a positive constant, $\tilde{y}(k) = y_r(k) - y(k)$, $l_1 = 0.382$, $l_2 = 0.618$, and d_1 and d_2 are positive constants.

Major results (1/11)

- Review of simulation results

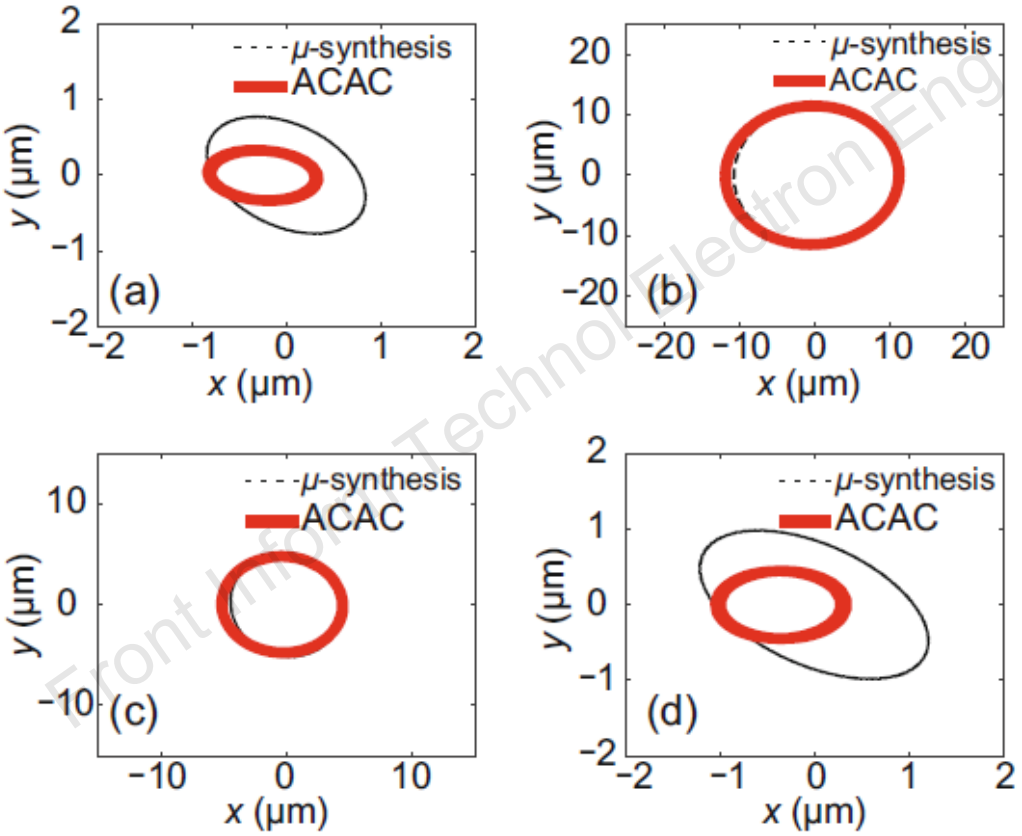

Fig. 4 Simulated rotor orbits at $\Omega = 7600\,\mathrm{r/min}$ under the μ-synthesis controller and characteristic model based ACAC: (a) dn$x$-dn$y$; (b) dm$x$-dm$y$; (c) dq$x$-dq$y$; (d) dd$x$-dd$y$

Major results (2/11)

- Review of experimental results

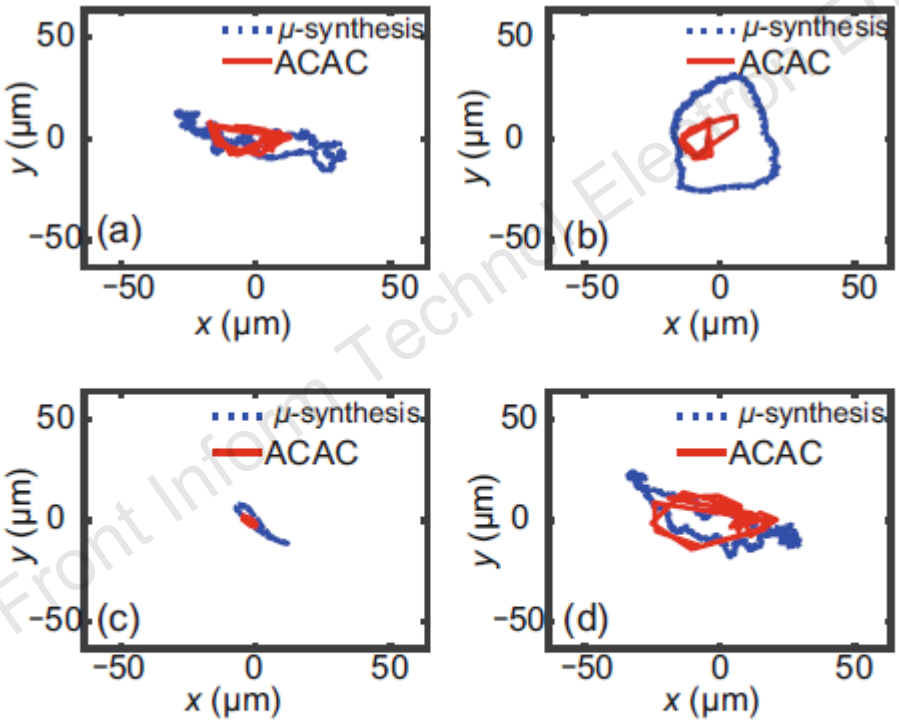

Fig. 5 Experimental rotor orbits at $\Omega = 7600$ r/min under the μ-synthesis controller and characteristic model based ACAC: (a) dn$x$-dn$y$; (b) dm$x$-dm$y$; (c) dq$x$-dq$y$; (d) dd$x$-dd$y$

Major results (3/11)

- Robustness with respect to plant uncertainties

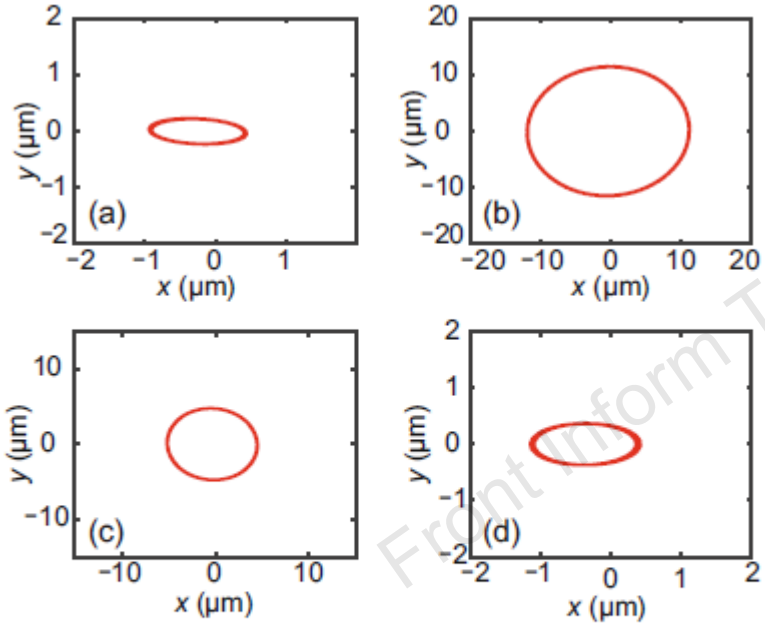

Fig. 6 Rotor orbits at $\Omega = 7600$ r/min of an emulated flywheel with $J_{\mathrm{p}} = 0.042$ kg·m^2 under characteristic model based ACAC laws: (a) dn$x$-dn$y$; (b) dm$x$-dm$y$; (c) dq$x$-dq$y$; (d) dd$x$-dd$y$

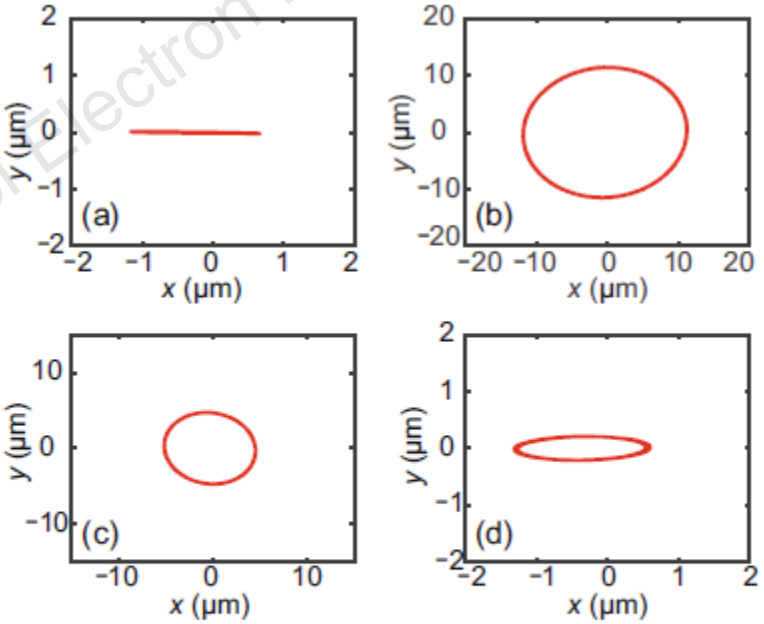

Fig. 7 Rotor orbits at $\Omega = 7600$ r/min of an emulated flywheel with $J_{\mathrm{p}} = 0.084$ kg·m^2 under characteristic model based ACAC laws: (a) dn$x$-dn$y$; (b) dm$x$-dm$y$; (c) dq$x$-dq$y$; (d) dd$x$-dd$y$

Major results (4/11)

- Robustness with respect to plant uncertainties

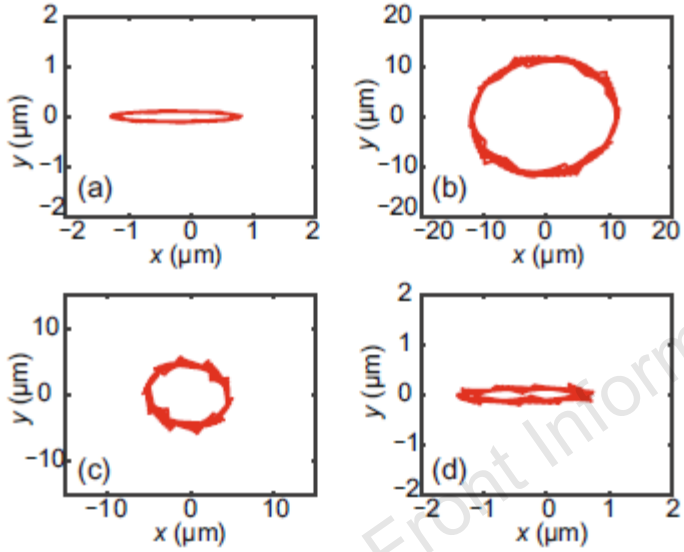

Fig. 8 Rotor orbits at $\Omega = 7600$ r/min of an emulated flywheel with $J_{\mathrm{p}} = 0.105$ kg·m^2 under characteristic model based ACAC laws: (a) dn$x$-dn$y$; (b) dm$x$-dm$y$; (c) dq$x$-dq$y$; (d) dd$x$-dd$y$

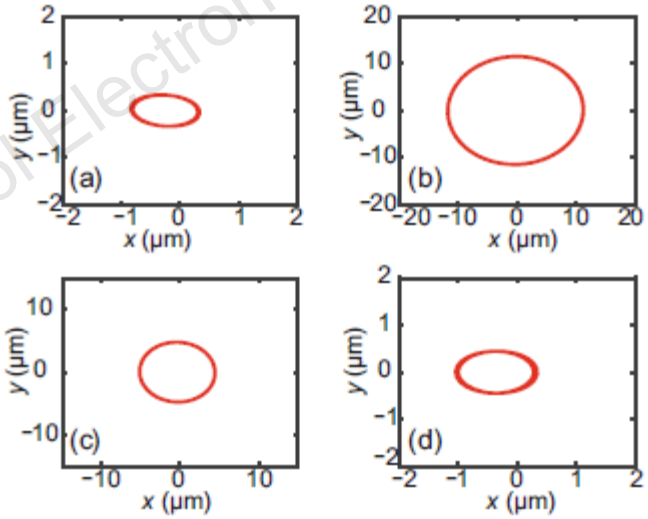

Fig. 9 Rotor orbits at $\Omega = 7600$ r/min of an emulated flywheel with $J_{\mathrm{p}} = 0.021$ kg·m^2 under characteristic model based ACAC laws: (a) dn$x$-dn$y$; (b) dm$x$-dm$y$; (c) dq$x$-dq$y$; (d) dd$x$-dd$y$

Major results (5/11)

- Robustness with respect to external disturbances

Constant disturbances:

Table 1 Peak values of the rotor displacements at $\Omega = 7600$ r/min of an emulated flywheel with $J_p = 0.021\,\mathrm{kg{\cdot}m^2}$ and Δi=0.1, 0.3, and 0.5 A, under characteristic model based ACAC laws

Location	Peak value (μm)		
	$\Delta i = 0.1$ A	$\Delta i = 0.3$ A	$\Delta i = 0.5$ A
dn$x$	25	74	122
dn$y$	42	124	207
dm$x$	41	95	152
dm$y$	45	110	176
dq$x$	37	98	159
dq$y$	31	84	137
dd$x$	33	98	162
dd$y$	25	73	121

Major results (6/11)

- Robustness with respect to external disturbances

Constant disturbances:

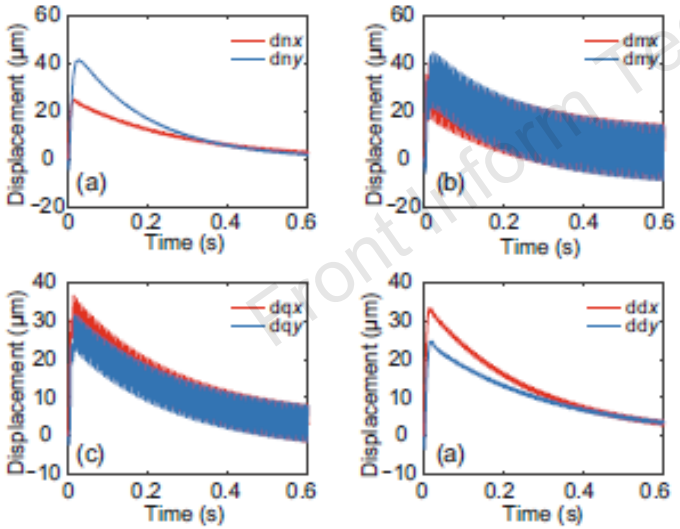

Fig. 10 Rotor displacements at $\Omega = 7600$ r/min of an emulated flywheel with $J_p = 0.021$ kg·m^2 and Δi=0.1 A, under characteristic model based ACAC laws: (a) NDE; (b) MID; (c) QTR; (d) DE

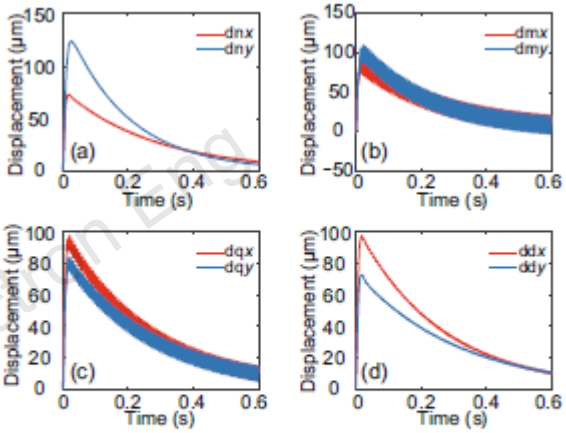

Fig. 11 Rotor displacements at $\Omega = 7600$ r/min of an emulated flywheel with $J_p = 0.021$ kg·m^2 and Δi=0.3 A, under characteristic model based ACAC laws: (a) NDE; (b) MID; (c) QTR; (d) DE

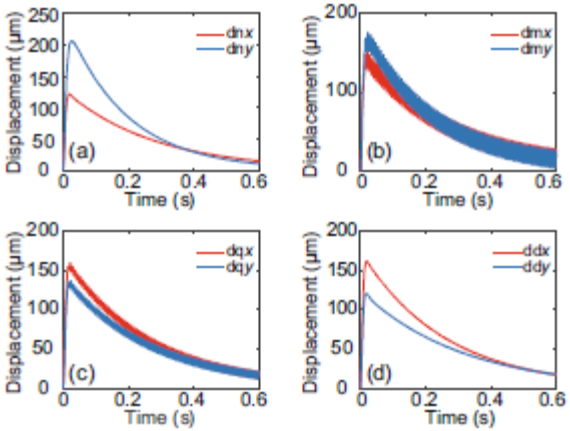

Fig. 12 Rotor displacements at $\Omega = 7600$ r/min of an emulated flywheel with $J_p = 0.021$ kg·m^2 and Δi=0.5 A, under characteristic model based ACAC laws: (a) NDE; (b) MID; (c) QTR; (d) DE

Major results (7/11)

- Robustness with respect to external disturbances

Constant disturbances:

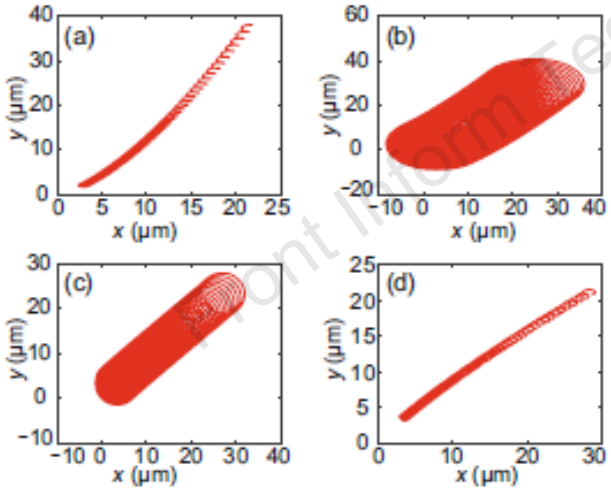

Fig. 13 Rotor orbits at $\Omega = 7600$ r/min of an emulated flywheel with $J_p = 0.021$ kg·m^2 and Δi=0.1 A, under characteristic model based ACAC laws: (a) dn$x$-dn$y$; (b) dm$x$-dm$y$; (c) dq$x$-dq$y$; (d) dd$x$-dd$y$

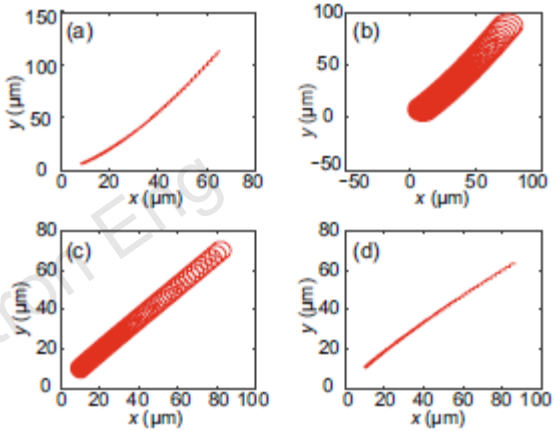

Fig. 14 Rotor orbits at $\Omega = 7600$ r/min of an emulated flywheel with $J_p = 0.021$ kg·m^2 and Δi=0.3 A, under characteristic model based ACAC laws: (a) dn$x$-dn$y$; (b) dm$x$-dm$y$; (c) dq$x$-dq$y$; (d) dd$x$-dd$y$

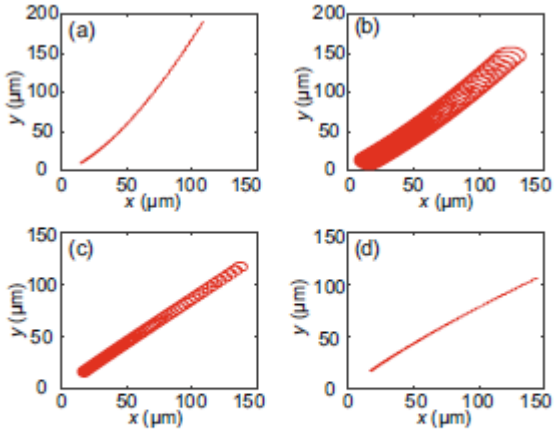

Fig. 15 Rotor orbits at $\Omega = 7600$ r/min of an emulated flywheel with $J_p = 0.021$ kg·m^2 and Δi=0.5 A, under characteristic model based ACAC laws: (a) dn$x$-dn$y$; (b) dm$x$-dm$y$; (c) dq$x$-dq$y$; (d) dd$x$-dd$y$

Major results (8/11)

- Robustness with respect to external disturbances

Sinusoidal disturbances:

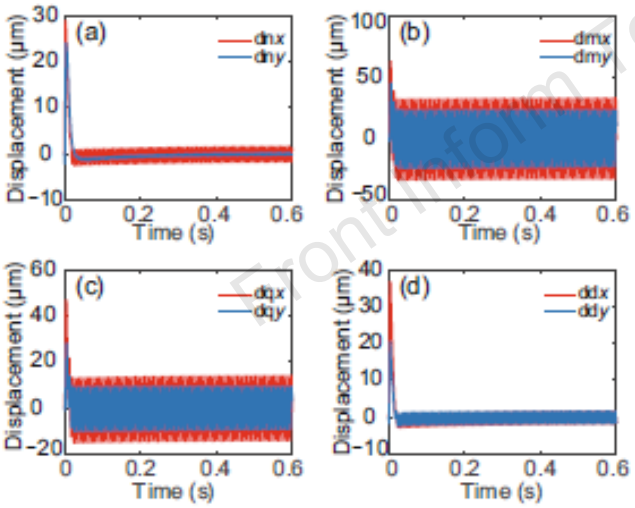

Fig. 16 Rotor displacements at $\Omega = 7600$ r/min of an emulated flywheel with $J_p = 0.021$ kg·m^2 and $\Delta i = 0.5\sin(\omega t)$, under characteristic model based ACAC laws: (a) NDE; (b) MID; (c) QTR; (d) DE

Table 2 Peak values of the rotor displacements at $\Omega = 7600$ r/min of an emulated flywheel with $J_p = 0.021$ kg·m^2 and $\Delta i = 0.5\sin(\omega t)$, under characteristic model based ACAC laws

Location	Peak value (μm)
dn$x$	29.1
dn$y$	24.2
dm$x$	63.2
dm$y$	45.3
dq$x$	47.2
dq$y$	28.1
dd$x$	37.0
dd$y$	20.5

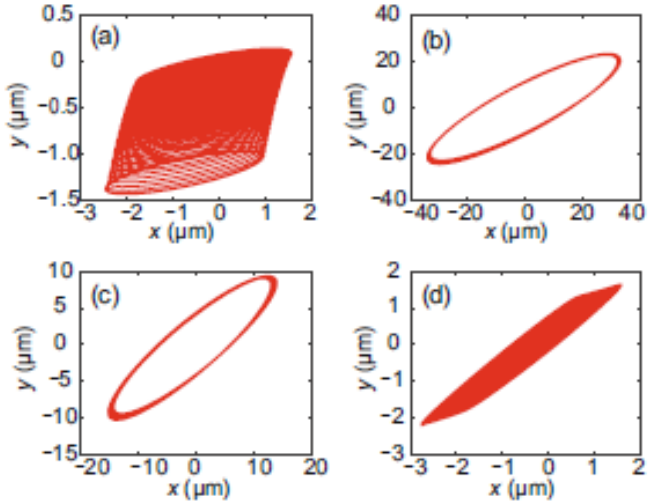

Fig. 17 Rotor orbits at $\Omega = 7600$ r/min of an emulated flywheel with $J_p = 0.021$ kg·m^2 and $\Delta i = 0.5\sin(\omega t)$, under characteristic model based ACAC laws: (a) dn$x$-dn$y$; (b) dm$x$-dm$y$; (c) dq$x$-dq$y$; (d) dd$x$-dd$y$

Major results (9/11)

- Robustness with respect to time delays

Control input delays:

Table 3 Peak values of the rotor displacements at $\Omega =$ 7600 r/min of an emulated flywheel with $J_p = 0.021$ kg·m^2, Δi=0.1 A, and control input delay $\tau = T_s$, under characteristic model based ACAC laws

Location	Peak value (μm)
dn$x$	25.2
dn$y$	41.7
dm$x$	41.1
dm$y$	44.5
dq$x$	36.8
dq$y$	31.6
dd$x$	33.7
dd$y$	24.8

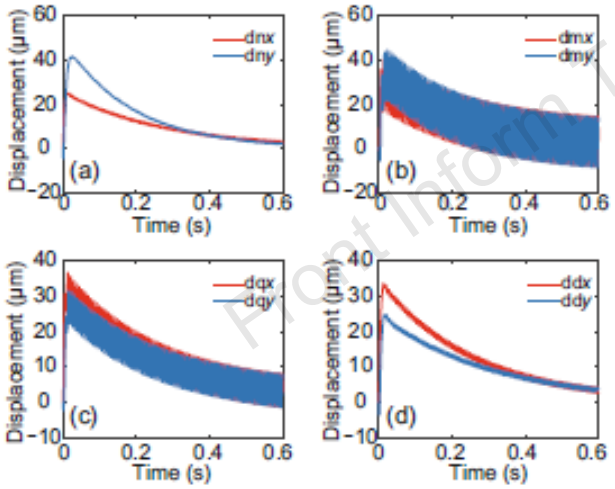

Fig. 18 Rotor displacements at $\Omega = 7600$ r/min of an emulated flywheel with $J_p = 0.021$ kg·m^2, Δi=0.1 A, and control input delay $\tau = T_s$, under characteristic model based ACAC laws: (a) NDE; (b) MID; (c) QTR; (d) DE

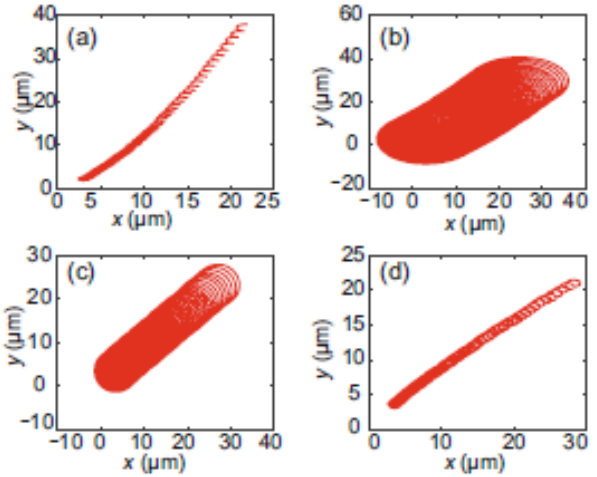

Fig. 19 Rotor orbits at $\Omega = 7600$ r/min of an emulated flywheel with $J_p = 0.021$ kg·m^2, Δi=0.1 A, and control input delay $\tau = T_s$, under characteristic model based ACAC laws: (a) dn$x$-dn$y$; (b) dm$x$-dm$y$; (c) dq$x$-dq$y$; (d) dd$x$-dd$y$

Major results (10/11)

- Robustness with respect to time delays

Sensor output delays:

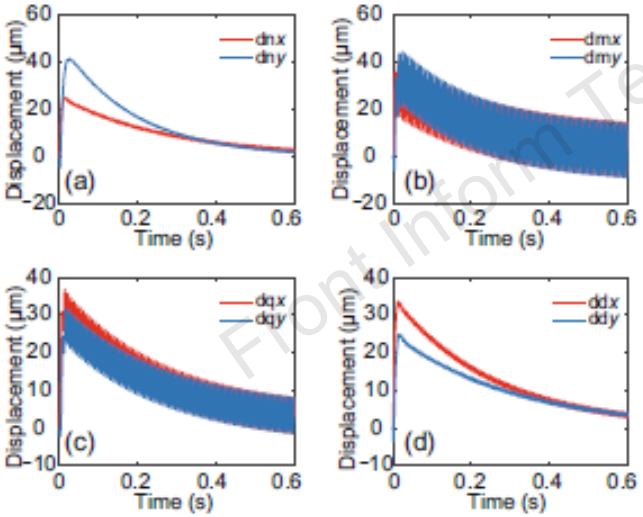

Fig. 20 Rotor displacements at $\Omega = 7600$ r/min of an emulated flywheel with $J_p = 0.021$ kg·m^2, Δi=0.1 A, and sensor output delay $\tau = T_s$, under characteristic model based ACAC laws: (a) NDE; (b) MID; (c) QTR; (d) DE

Table 4 Peak values of the rotor displacements at $\Omega = 7600$ r/min of an emulated flywheel with $J_p = 0.021$ kg·m^2, Δi=0.1 A, and sensor output delay $\tau = T_s$, under characteristic model based ACAC laws

Location	Peak value (μm)
dn$x$	25.3
dn$y$	41.8
dm$x$	41.1
dm$y$	44.3
dq$x$	36.8
dq$y$	31.6
dd$x$	33.7
dd$y$	24.8

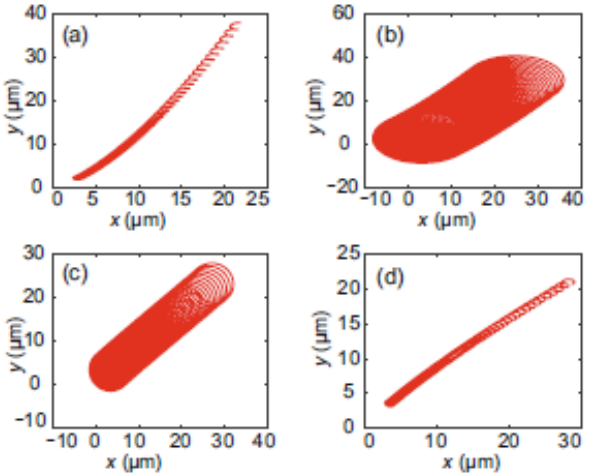

Fig. 21 Rotor orbits at $\Omega = 7600$ r/min of an emulated flywheel with $J_p = 0.021$ kg·m^2, Δi=0.1 A, and sensor output delay $\tau = T_s$, under characteristic model based ACAC laws: (a) dn$x$-dn$y$; (b) dm$x$-dm$y$; (c) dq$x$-dq$y$; (d) dd$x$-dd$y$

Major results (11/11)

- Robustness with respect to time delays

Delays at control inputs and sensor outputs:

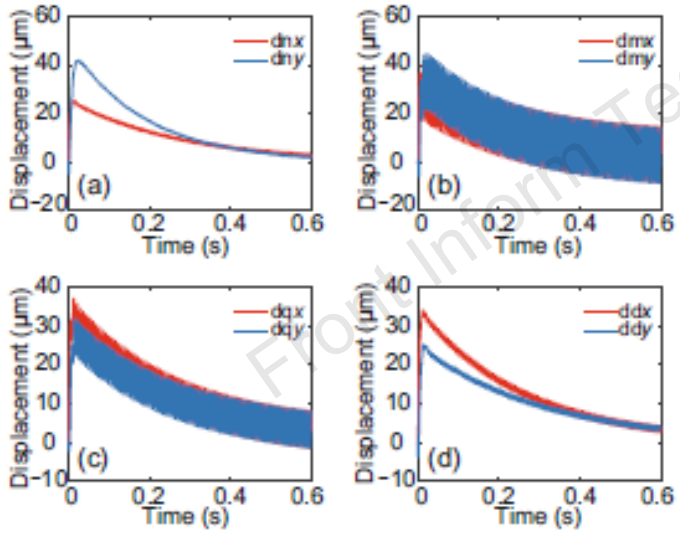

Fig. 22 Rotor displacements at $\Omega = 7600$ r/min of an emulated flywheel with $J_p = 0.021$ kg·m^2, Δi=0.1 A, control input delay $\tau = T_s$, and sensor output delay $\tau = T_s$, under characteristic model based ACAC laws: (a) NDE; (b) MID; (c) QTR; (d) DE

Table 5 Peak values of the rotor displacements at $\Omega = 7600$ r/min of an emulated flywheel with $J_p = 0.021$ kg·m^2, Δi=0.1 A, control input delay $\tau = T_s$, and sensor output delay $\tau = T_s$, under characteristic model based ACAC laws

Location	Peak value (μm)
dn$x$	25.3
dn$y$	41.8
dm$x$	41.4
dm$y$	44.6
dq$x$	36.9
dq$y$	31.8
dd$x$	34.0
dd$y$	25.1

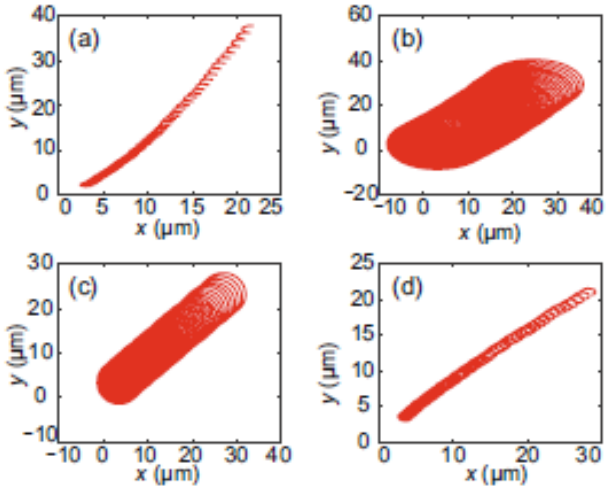

Fig. 23 Rotor orbits at $\Omega = 7600$ r/min of an emulated flywheel with $J_p = 0.021$ kg·m^2, Δi=0.1 A, control input delay $\tau = T_s$, and sensor output delay $\tau = T_s$, under characteristic model based ACAC laws: (a) dn$x$-dn$y$; (b) dm$x$-dm$y$; (c) dq$x$-dq$y$; (d) dd$x$-dd$y$

Conclusions

1. The robustness of the characteristic model based all-coefficient adaptive control (ACAC) on an AMB suspended energy storage flywheel test rig with respect to plant uncertainties, external disturbances, and time delay is investigated.

2. The experimental platform for the AMB suspended energy storage flywheel, developed from an existing flexible rotor-AMB test rig in the ROMAC Laboratory at the University of Virginia, has been reviewed.

3. The rotor behaviors of the flywheel emulation platform under the characteristic model based ACAC have been briefly presented.

4. The performances of the closed-loop flywheel AMB systems with plant uncertainties, external disturbances, and time delay have been tested in the simulations.

5. Extensive and systematic simulations demonstrated that the characteristic model based ACAC possesses considerable robustness with respect to plant uncertainties, external disturbances, and time delay.

References

Di L, Lin ZL, 2014. Control of a flexible rotor active magnetic bearing test rig: a characteristic model based all-coefficient adaptive control approach. *Contr Theor Technol*, 12(1):1-12. https://doi.org/10.1007/s11768-014-0184-0

Lyu XJ, Di L, Yoon SY, et al., 2016. A platform for analysis and control design: emulation of energy storage flywheels on a rotor-AMB test rig. *Mechatronics*, 33:146-160. https://doi.org/10.1016/j.mechatronics.2015.12.007

Lyu XJ, Di L, Lin ZL, et al., 2018. Characteristic model based all-coefficient adaptive control of an AMB suspended energy storage flywheel test rig. *Sci China Inform Sci*, 61(11):112204. https://doi.org/10.1007/s11432-017-9327-0

Wu HX, Hu J, Xie YC, 2007. Characteristic model-based all-coefficient adaptive control method and its applications. *IEEE Trans Syst Man Cybern Part C* (*Appl Rev*), 37(2):213-221. https://doi.org/10.1109/TSMCC.2006.887004

Wu HX, Hu J, Xie YC, 2009. Characteristic Model-Based and Intelligent Adaptive Control. Science and Technology Press of China, Beijing, China (in Chinese).